# Last time | Dipole Picture of DIS
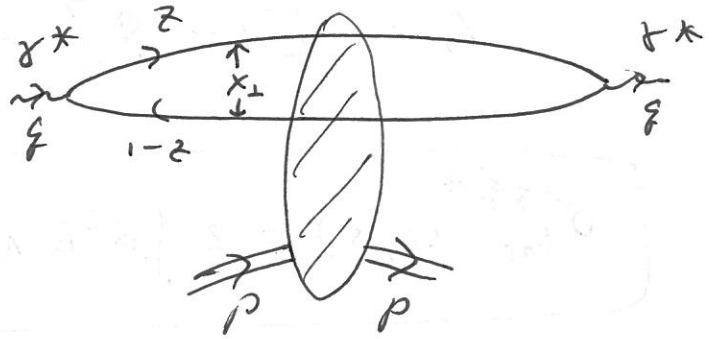


$$\sigma_{tot}^{\gamma^* A}(x, Q^2) = \int \frac{d^2 x_\perp}{4\pi} \int_0^1 \frac{dz}{z(1-z)} \left| \Psi^{\gamma^* \to q\bar{q}}(\underline{x}, z) \right|^2 \sigma_{tot}^{q\bar{q}A}(\underline{x}, S)$$

$\Psi^{\gamma^* \to q\bar{q}}(\underline{x}, z) \sim$ known

## Structure functions:

$$F_2 = \frac{Q^2}{4\pi^2 \alpha_{EM}} \left( \sigma_T^{\gamma^* A} + \sigma_L^{\gamma^* A} \right)$$

$$2x F_1 = \frac{Q^2}{4\pi^2 \alpha_{EM}} \sigma_T^{\gamma^* A}$$

( In the naive Parton Model $F_2 = 2x F_1 \Rightarrow$

$\Rightarrow \sigma_L^{\gamma^* A}$ is small. )

$\leadsto$ Need to find $\sigma^{q\bar{q}A}(\underline{x}, s) \sim$ QCD is there.

**Def.** $\boxed{N(\underline{x}, \underline{b}, s) = \text{Im}\, A(\underline{x}, \underline{b}, s)}$

$A = i[1 - \hat{S}] \Rightarrow \boxed{N(\underline{x}, \underline{b}, s) = 1 - \text{Re}\, \hat{S}(\underline{x}, \underline{b}, s)}$

$\boxed{\sigma_{tot}^{q\bar{q}A}(\underline{x}, s) = 2 \int d^2b \, N(\underline{x}, \underline{b}, s)}$

## Glauber – Gribov – Mueller multiple rescattering formula

Imagine a single-nucleon target

$$\boxed{\sigma^{q\bar{q}N} \simeq \frac{2\pi \, d_s^2 \, C_F}{N_c} x_\perp^2 \ln \frac{1}{x_\perp^2 \Lambda^2}}$$



$+ \ldots$

(perm's)
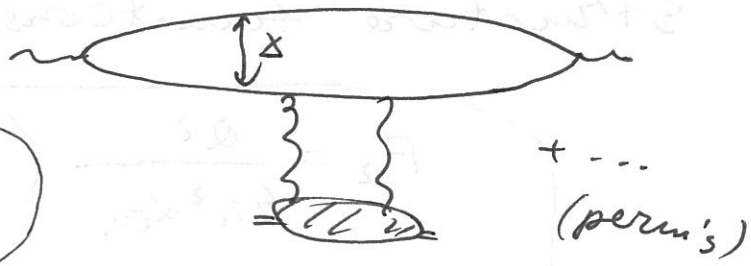
(Treating the proton as a large dipole of transverse size $\frac{1}{\Lambda} \gg x_\perp$.)

zero-transverse-size dipoles do not interact with the nucleus (they have zero scattering cross section) and so such configurations do not contribute to the DIS structure functions.

Fourier-transforming Eq. (4.19) into transverse coordinate space yields

$$\Psi_L^{\gamma^* \to q\bar{q}}(\vec{x}_\perp, z) = \frac{eZ_f}{2\pi}[z(1-z)]^{3/2}\, \delta_{ij}\, 2Q(1 - \delta_{\sigma\sigma'})K_0(x_\perp a_f), \qquad (4.20)$$

so that the longitudinal wave function squared, again with all summations performed, is (Bjorken, Kogut, and Soper 1971, Nikolaev and Zakharov 1991)

$$|\Psi_L^{\gamma^* \to q\bar{q}}(\vec{x}_\perp, z)|^2 = 2N_c \sum_f \frac{\alpha_{EM}Z_f^2}{\pi} 4Q^2 z^3(1-z)^3 \left[K_0(x_\perp a_f)\right]^2. \qquad (4.21)$$

To obtain the phase-space integral in Eqs. (4.6) or (4.12) we remember that the two-particle momentum phase space given in Eq. (1.82) is (remembering that in our case the quarks are not identical)

$$\int \frac{dz}{2z(1-z)} \frac{d^2 k_\perp}{(2\pi)^3}. \qquad (4.22)$$

After Fourier-transforming the wave function into transverse coordinate space the integral becomes

$$\int \frac{dz}{2z(1-z)} \frac{d^2 x_\perp}{2\pi}, \qquad (4.23)$$

in agreement with Eqs. (4.6) and (4.12).

We have now completed the calculation of the QED part of DIS in the dipole picture. Equations (4.18) and (4.21), when used in Eq. (4.12), give us the transverse and longitudinal DIS cross sections, which, in turn, when used in Eqs. (4.10) and (4.11) give us the structure functions. The interesting physics of strong interactions is contained in the dipole–nucleus scattering cross section $\sigma_{tot}^{q\bar{q}A}(\vec{x}_\perp, Y)$: most of this chapter is dedicated to calculating this quantity.

## 4.2 Glauber–Gribov–Mueller multiple-rescatterings formula

We begin by employing Eq. (3.119a) to rewrite the total dipole–nucleus scattering cross section as

$$\sigma_{tot}^{q\bar{q}A}(\vec{x}_\perp, Y) = 2 \int d^2b \, N(\vec{x}_\perp, \vec{b}_\perp, Y), \qquad (4.24)$$

where $N(\vec{x}_\perp, \vec{b}_\perp, Y)$ is the imaginary part of the forward scattering amplitude for a dipole of transverse size $\vec{x}_\perp$ interacting with the nucleus at impact parameter $\vec{b}_\perp$ and with net rapidity interval $Y$. Hence to find the cross section $\sigma_{tot}^{q\bar{q}A}$ we need to calculate $N(\vec{x}_\perp, \vec{b}_\perp, Y)$.

To find $N(\vec{x}_\perp, \vec{b}_\perp, Y)$ let us consider the following (Glauber) model. Assume that the nucleus is very large and dilute and is made out of $A \gg 1$ independent nucleons, where $A$ is
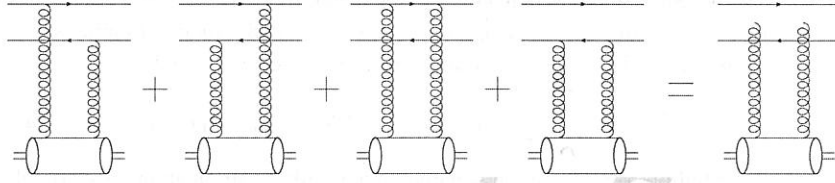
Fig. 4.3. The four diagrams contributing to dipole interaction with a single nucleon at the lowest nontrivial (two-gluon) order in the high energy approximation and an abbreviated notation for their sum.

the atomic number of the nucleus.[1] Any correlations between the nucleons are suppressed by powers of the large parameter $A$: hence our approximation corresponds to summing the leading powers of $A$. In evaluating the forward dipole–nucleus scattering amplitude $N(\vec{x}_\perp, \vec{b}_\perp, Y)$ we will follow the strategy originally outlined by Glauber and by Gribov (Glauber 1955, Franco and Glauber 1966, Gribov 1969b, Glauber and Matthiae 1970, Gribov 1970) and implemented in QCD by Mueller (1990).

### 4.2.1 Scattering on one nucleon

First we consider the case when the dipole interacts with only one nucleon in the nucleus. Assuming that the interaction is entirely perturbative, we see that the lowest-order contribution to the forward high energy scattering amplitude comes from a two-gluon exchange. The relevant diagrams are shown in Fig. 4.3. This lowest-order scattering process was calculated in Sec. 3.2. Employing the results of that section (see Eq. (3.25)) we can write down the total dipole–nucleon cross section as

$$\sigma^{q\bar{q}N} \approx \frac{2\pi \alpha_s^2 C_F}{N_c} x_\perp^2 \ln \frac{1}{x_\perp^2 \Lambda^2}. \tag{4.25}$$

In arriving at Eq. (4.25) we have assumed that the dipole is perturbatively small, $x_\perp \ll 1/\Lambda_{QCD}$, and that the nucleon can be modeled as another dipole of transverse size $1/\Lambda \gg x_\perp$, with $\Lambda$ some soft QCD scale of order $\Lambda_{QCD}$. We have also assumed that the nucleus is sufficiently large that the cross section does not depend on the dipole's orientation in the transverse plane, over which we therefore average.

At the same two-gluon order the unintegrated gluon distribution function of the nucleon can be found using Eq. (3.92) with the lowest-order BFKL Green function (3.59). This gives

$$\phi_{LO}^{onium}(x, k_\perp^2) = \frac{\alpha_s C_F}{\pi} \frac{2}{k_\perp^2}, \tag{4.26}$$

where we have assumed that $k_\perp \gg \Lambda$. The factor 2 on the right-hand side of Eq. (4.26) simply counts the number of quarks in the dipole representing the nucleon. It should be

---

[1]  Strictly speaking $A$ is called the mass number of the nucleus; nevertheless, we will follow the standard jargon in the high energy field and refer to it as the atomic number.

replaced by $N_c$ if one wanted to model the nucleon more realistically, as consisting of $N_c$ valence quarks. Using Eq. (3.93) the corresponding lowest-order gluon distribution of an onium (a nucleon) turns out to be

$$xG_{LO}^{onium}(x, Q_\perp^2) = \frac{\alpha_s C_F}{\pi} 2 \ln \frac{Q^2}{\Lambda^2}. \tag{4.27}$$

Comparing Eq. (4.27) and Eq. (4.25), we can rewrite the latter as

$$\sigma^{q\bar{q}N} \approx \frac{\alpha_s \pi^2}{N_c} x_\perp^2 xG_N\left(x, \frac{1}{x_\perp^2}\right), \tag{4.28}$$

where $xG_N$ is the gluon distribution in the nucleon (presently modeled as an onium).[2] Equation (4.28) has an advantage over Eq. (4.25): it is valid for any nonperturbative gluon distribution in the nucleon and is therefore more general. We will use these equations interchangeably, though.

To find the dipole–nucleus scattering cross section at a given impact parameter we need to average the dipole–nucleon scattering amplitude over all possible positions of the nucleon inside the nucleus and to sum over the $A$ nucleons in the nucleus, all of which may participate in the interaction. We have

$$\frac{d\sigma_{LO}^{q\bar{q}A}}{d^2b} = \int db_3' d^2b_\perp' \rho_A(\vec{b}_\perp - \vec{b}_\perp', b_3') \frac{d\sigma^{q\bar{q}N}}{d^2b'}, \tag{4.29}$$

where $db_3' d^2b_\perp' = d^3b$ is the three-dimensional volume element and $\rho_A(\vec{b}_\perp, b_3)$ is the nucleon number density, with $\vec{b}_\perp = (b_1, b_2)$. In a simplified model, of the nucleus has a constant nucleon number density $\rho_A = A/V$, where $V$ is the volume of the nucleus in its rest frame. In the general case $\rho_A(\vec{b}_\perp, b_3)$ is given by the Woods–Saxon parametrization of the nuclear density (Woods and Saxon 1954).

Equation (4.29) gives the cross section for a dipole at impact parameter $\vec{b}_\perp$ scattering on a nucleon at impact parameter $\vec{b}_\perp - \vec{b}_\perp'$ (where $\vec{b}_\perp'$ is its transverse distance from the dipole), convoluted with the nucleon density $\rho$, which, in turn, is proportional to the probability of finding a nucleon at $\vec{b}_\perp - \vec{b}_\perp'$ (see Fig. 4.4). To simplify Eq. (4.29) we note that the perturbative scattering cross section falls off as $d\sigma^{q\bar{q}N}/d^2b' \sim 1/b_\perp'^4$ at large impact parameter, as can be seen for instance from Eq. (3.139) in Exercise 3.3 (after averaging over the azimuthal orientations of one dipole; this mimics an unpolarized nucleon, without any preferred direction). At nonperturbatively large impact parameter $b_\perp' \gtrsim 1/\Lambda_{QCD}$ one expects an even steeper falloff, $d\sigma^{q\bar{q}N}/d^2b' \sim \exp(-2m_\pi b_\perp')$ (cf. Eq. (3.113)). Hence the cross section $d\sigma^{q\bar{q}N}/d^2b'$ is localized at small impact parameters $b_\perp' \lesssim 1/\Lambda_{QCD}$.

In the large-$A$ approximation that we are employing, one assumes that the nuclear wave function and hence the density $\rho_A(\vec{b}_\perp, b_3)$ does not change significantly over distances of order $1/\Lambda_{QCD}$, which is small compared with the size of the nucleus, so that the nucleon has an approximately equal probability of being anywhere within this transverse range.

---

[2] We would like to stress here that in order to conform to the standard notation we write the gluon distribution with Bjorken $x$ in its argument, but throughout this section the gluon distribution is taken at the lowest (two-gluon) order and is therefore $x$-independent.

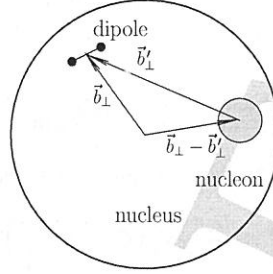132    *Dipole approach to high parton density QCD*



Fig. 4.4. The geometry of dipole–nucleus scattering in the transverse coordinate plane. To illustrate the notation of Eq. (4.29) the diagram places the dipole far from the nucleus: in reality $b'_\perp \lesssim 1/\Lambda_{QCD}$.

Therefore, for large nuclei we can approximate $\rho_A(\vec{b}_\perp - \vec{b}'_\perp, b'_3)$ as $\rho_A(\vec{b}_\perp, b'_3)$ and recast Eq. (4.29) by integrating over $b'_\perp$ as

$$\frac{d\sigma_{LO}^{q\bar{q}A}}{d^2b} = T(\vec{b}_\perp)\sigma^{q\bar{q}N}, \quad = 2N \tag{4.30}$$

where we have defined the *nuclear profile function* $T(\vec{b}_\perp)$ by

$$T(\vec{b}_\perp) \equiv \int_{-\infty}^{\infty} db_3 \rho_A(\vec{b}_\perp, b_3). \tag{4.31}$$

For a spherical nucleus of radius $R$ with constant nucleon number density $\rho_A = A/V$ one has $T(\vec{b}_\perp) = 2\rho_A\sqrt{R^2 - \vec{b}_\perp^2}$.

Comparing Eq. (4.30) with Eq. (4.24) and employing Eq. (4.28) we obtain

$$N_{LO}(\vec{x}_\perp, \vec{b}_\perp, Y) = \frac{\alpha_s \pi^2}{2N_c} T(\vec{b}_\perp) x_\perp^2 x G_N\left(x, \frac{1}{x_\perp^2}\right)$$

$$= \frac{\pi \alpha_s^2 C_F}{N_c} T(\vec{b}_\perp) x_\perp^2 \ln\frac{1}{x_\perp \Lambda}, \tag{4.32}$$

where in the last line we have modeled the nucleon by a single quark with gluon distribution

$$x G(x, Q_\perp^2) = \frac{\alpha_s C_F}{\pi} \ln\frac{Q^2}{\Lambda^2}.$$

We now have the forward dipole–nucleus scattering amplitude for the case when only one nucleon in the nucleus interacts with the dipole. This case has a problem akin to that of linear BFKL evolution: if we increase the dipole size $x_\perp$ in Eq. (4.32), at some point we get $N_{LO} > 1$, violating the *black-disk limit*, which states that

$$N(\vec{x}_\perp, \vec{b}_\perp, Y) \leq 1 \tag{4.33}$$
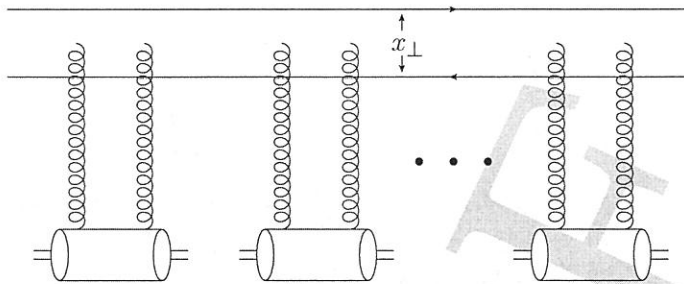
(see Eq. (B.37) in Appendix B).

Fig. 4.5. Dipole–nucleus scattering in the Glauber–Gribov–Mueller approximation in the Feynman gauge. The disconnected gluon lines at the top denote the sum over all possible connections of the gluon lines to the dipole, as depicted in Fig. 4.3.

Let us stress again here that the transverse dipole size $x_\perp$ is preserved in high energy interactions. This makes the $S$-matrix diagonal not only in the impact parameter $\vec{b}_\perp$, as we saw in Eqs. (3.119) and also in Appendix B, but also in the dipole size $\vec{x}_\perp$. Therefore, the relations (3.119) between the cross sections and the $S$-matrix can also be written down for dipole–nucleus scattering with a fixed dipole size $\vec{x}_\perp$. The unitarity conditions (the optical theorem), which in momentum space are written as complicated convolutions (see e.g. Eq. (B.19)), become simple products of the amplitudes in $(\vec{x}_\perp, \vec{b}_\perp)$-space (see e.g. Eq. (B.30)). For this reason we think of color dipoles (or any other objects in the transverse coordinate representation) as the correct degrees of freedom for high energy scattering.

### 4.2.2  Scattering on many nucleons

When the probability of interaction with one nucleon becomes large, interactions with multiple nucleons also becomes likely and should be taken into account. Now we will see how multiple rescatterings of the dipole on different nucleons cure the problem of black-disk-limit violation by Eq. (4.32).

Let us consider the case when any number of nucleons can interact, restricting the interaction with each nucleon to the lowest nontrivial order. For this calculation we will be working in the standard Feynman perturbation theory using the Lorenz $\partial_\mu A^\mu = 0$ (Feynman) gauge. (Once we have separated the DIS cross section into the light cone wave function squared and the dipole–nucleus cross section, we can calculate the latter using any technique that is convenient.) We start by stating the diagrammatic answer for the many-nucleon interaction case: in the Feynman gauge, the dipole–nucleus interaction becomes a series of successive independent dipole–nucleon rescatterings, as shown in Fig. 4.5. There each nucleon (denoted by an oval at the bottom, just as in Fig. 4.3) interacts with the dipole via a two-gluon exchange: the disconnected gluon lines at the top of the diagram denote all possible connections to the quark and the antiquark lines in the dipole, as defined in Fig. 4.3.

The diagram in Fig. 4.5 implies that in the covariant gauge there is no direct "cross-talk" between the nucleons and that all the nucleons interact sequentially in the order in which
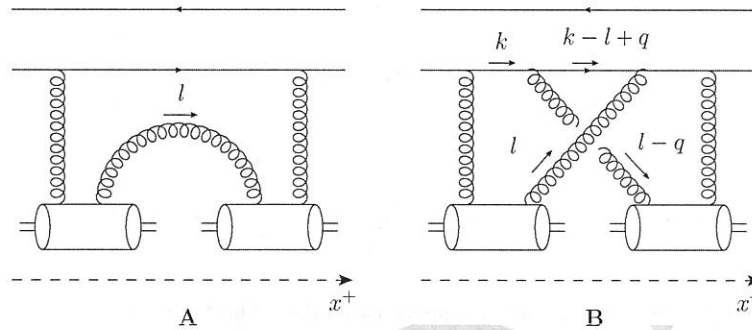
Fig. 4.6. Examples of diagrams that can be neglected for dipole–nucleus scattering in the covariant (Feynman) gauge.
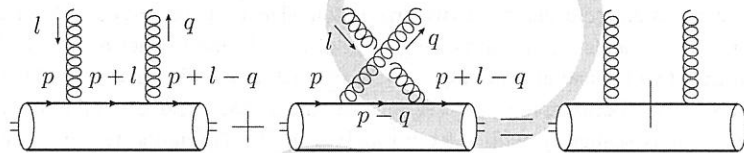


Fig. 4.7. Diagrammatic illustration that for a color-singlet object such as a nucleon, the coupling of two gluons to a single quark line is equivalent to the coupling of each gluon to a quark line that is on mass shell both before and after the quark–gluon interaction. The solid vertical line in the rightmost graph indicates an effective cut.

the dipole encounters them, i.e., according to their ordering along the $x^+$-axis. The dipole–nucleon interactions in the covariant gauge of Fig. 4.5 are localized inside the nucleons, on distance scales much shorter than the nuclear radius. While for a large dilute nucleus these assertions seem natural, we still need to prove them. To do so, it is convenient to change the frame slightly by giving the nucleus a slight boost, so that it moves along the light cone in the minus direction with a large $P^-$ momentum. At the same time the boost preserves the virtual photon's motion along the plus light cone, with four-momentum as shown in Eq. (4.1). Thus both the dipole and nucleus in this new frame move along their respective light cones, as shown in Fig. 4.8. In the calculations below we will assume that the gluon–nucleon coupling is perturbatively small.

To illustrate why the graphs in Fig. 4.5 dominate the scattering, let us show that the diagrams in Fig. 4.6, demonstrating "cross-talk" (A) and the violation of $x^+$-ordering (B), are suppressed and can be neglected. Before we do that, let us carry out a simple exercise elucidating the nature of the coupling of two gluons to a nucleon. Consider two gluons coupling to a quark line in a nucleon, as shown in Fig. 4.7. This can be a part of any diagram in Figs. 4.6 and 4.5. Note that one has to include a crossed diagram, as illustrated in Fig. 4.7. Since the nucleon is a color singlet, the color factors of the two graphs on the left in Fig. 4.7 are identical (say, owing to a color trace), so that the difference between the two diagrams is only in the propagators for the internal quark line. Adding the two propagators (using the momentum labels from Fig. 4.7) and remembering that $p^-$ is the largest momentum in the
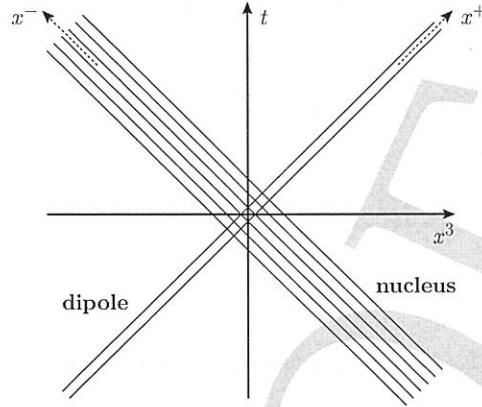
Fig. 4.8. Space–time picture of the dipole–nucleus scattering.

problem, we obtain

$$\frac{i(\not p + \not l + m_q)}{(p+l)^2 - m_q^2 + i\epsilon} + \frac{i(\not p - \not q + m_q)}{(p-q)^2 - m_q^2 + i\epsilon}$$

$$\approx i\not p \left( \frac{1}{p^- l^+ + i\epsilon} + \frac{1}{-p^- q^+ + i\epsilon} \right) = i\not p\, 2\pi i \delta(p^- l^+). \qquad (4.34)$$

We have used the fact that the outgoing quark is on mass shell, $(p + l - q)^2 = m_q^2$, so that $q^+ = l^+$ with eikonal accuracy (see Sec. 3.2 for similar estimates). We conclude that (with eikonal accuracy) $l^+ = q^+ = 0$. The $\delta$-function in Eq. (4.34) puts the internal quark line in the leftmost of Fig. 4.7 on mass shell. The result (4.34) can be summarized by replacing the internal quark line by the cut line, as shown in the rightmost graph of Fig. 4.7: the cut enforces $l^+ = 0$. What is essential to us is that neither gluon carries any plus momentum.

Now we are ready to evaluate the diagrams in Fig. 4.6. Note that, owing to the large size of the nucleus we are considering, even after the boost the nucleus is still somewhat spread out in the $x^+$-direction, as demonstrated in Fig. 4.8, where different nucleons correspond to different straight lines parallel to the $x^-$ light cone. Hence each nucleon in the nucleus is located at a different $x^+$ coordinate. We thus need to Fourier-transform the diagrams in Fig. 4.6 into coordinate $x^+$-space by integrating over $l^-$.

Starting with Fig. 4.6A we see that the $l^-$-dependence can be contained only in the propagator of the gluon carrying momentum $l$ that is exchanged between the nucleons there. However, as we have just shown when considering the diagrams in Fig. 4.7, $l^+ = 0$ with eikonal accuracy, so that the diagram in Fig. 4.6A is proportional to

$$\int_{-\infty}^{\infty} dl^- \frac{e^{-il^- \Delta x^+}}{l^2 + i\epsilon} \approx \int_{-\infty}^{\infty} dl^- \frac{e^{-il^- \Delta x^+}}{-\vec{l}_\perp^2} = 0 \qquad (4.35)$$
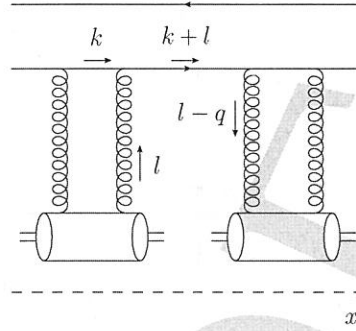
Fig. 4.9. Forward amplitude for a dipole scattering on two nucleons.

for nonzero light cone separations between the two nucleons, i.e., $\Delta x^+ \neq 0$. Hence diagram A is negligible in the covariant gauge in which we are working.[3] Let us stress that in arriving at the result (4.35) we have restricted ourselves to $l^- \ll p^-$: if we relaxed this constraint then the integral in Eq. (4.35) would be nonzero, though it would still be suppressed for large atomic numbers $A$ (Kovchegov 1997).

Similarly, in Fig. 4.6B one has $l^+ = q^+ = 0$, so that the $l^-$-dependence can be contained only in the quark propagator of the $(k - l + q)$-line. Since the light cone momentum of the quark $k^+$ is large, we see that the diagram in Fig. 4.6B is proportional to

$$\int_{-\infty}^{\infty} dl^- \frac{e^{-il^- \Delta x^+}}{(k-l+q)^2 + i\epsilon} \approx \int_{-\infty}^{\infty} dl^- \frac{e^{-il^- \Delta x^+}}{k^+(k^- - l^- + q^-) - (\vec{k}_\perp - \vec{l}_\perp + \vec{q}_\perp)^2 + i\epsilon} = 0$$

(4.36)

for $\Delta x^+ > 0$, as the pole of the propagator is in the upper half-plane while the contour needs to be closed in the lower half-plane. For $\Delta x^+ < 0$ the integral in Eq. (4.36) is not zero, but then we would obtain zero from the integral over the minus momentum carried by the other pair of $t$-channel gluon lines. We thus can neglect diagram B as well.

The arguments used in proving that diagrams A and B in Fig. 4.6 are zero can be generalized to more complicated diagrams in the same general categories. We have succeeded in demonstrating that in covariant gauge and in the approximation of two gluon exchanges per nucleon the dipole–nucleus interaction is given by the graphs in Fig. 4.5. We now need to resum these diagrams. To do this, we first consider dipole scattering on two nucleons ordered in $x^+$, as shown in Fig. 4.9. Unlike the diagram in Fig. 4.6B, the graph in Fig. 4.9 has the correct $x^+$-ordering of the nucleons. Instead of giving zero it yields (note that $k^-$ is very small for a quark on a plus light cone)

$$\int_{-\infty}^{\infty} \frac{dl^-}{2\pi} \frac{ie^{-il^- \Delta x^+}}{(k+l)^2 + i\epsilon} \approx \int_{-\infty}^{\infty} \frac{dl^-}{2\pi} \frac{ie^{-il^- \Delta x^+}}{k^+l^- - (\vec{k}_\perp + \vec{l}_\perp)^2 + i\epsilon} = \frac{1}{k^+},$$

(4.37)

[3] Note that diagram in Fig. 4.6A is nonzero in the $A^- = 0$ light cone gauge even in the eikonal approximation.
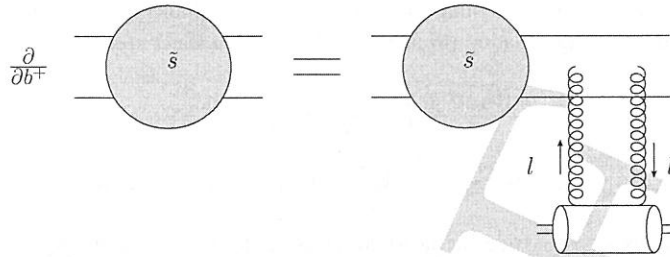
Fig. 4.10. Diagrammatic representation of Eq. (4.40) resumming all the diagrams from Fig. 4.5.

where at the end of the calculation we have neglected the phase of the exponential since it is proportional to $\Delta x^+/k^+ \sim 1/(k^+ p^-)$, which is suppressed by the center-of-mass energy. It is important to note that in picking up the pole in Eq. (4.37) we put the propagator of the quark carrying momentum $k + l$ on mass shell. Therefore, the diagram factorizes into a product of two independent dipole–nucleon scatterings; the quark and the antiquark in the dipole effectively go on shell between the scatterings. (The factor $1/k^+$ left in Eq. (4.37) serves to normalize the dipole–nucleon cross section for the nucleon on the right.) The numerator of the quark propagator can be absorbed into two separate scattering amplitudes using the property that (neglecting the quark mass) $\not{k} + \not{l} = \sum_\sigma u_\sigma(k + l)\bar{u}_\sigma(k + l)$: the factor $u_\sigma(k + l)$ is absorbed into one amplitude, while $\bar{u}_\sigma(k + l)$ is absorbed into the other. Comparing this result with the standard normalization factor for the $2 \to 2$ cross section at high energy (see Eqs. (B.22) and (B.23)), we conclude that to resum the diagrams in Fig. 4.5 we simply need to iterate the dipole–nucleus cross section.

Define the forward matrix element of the $S$-matrix for the dipole–nucleus scattering by (cf. Eq. (B.34))

$$S(\vec{x}_\perp, \vec{b}_\perp, Y) = 1 - N(\vec{x}_\perp, \vec{b}_\perp, Y). \tag{4.38}$$

Suppressing the arguments $\vec{b}_\perp$ and $Y$, we can define the $S$-matrix (the "propagator") $s(\vec{x}_\perp, b^+)$ for a dipole to travel through the nucleus up to a point $b^+$, so that $S(\vec{x}_\perp) = s(\vec{x}_\perp, L)$ with $b^+ \in (0, L)$ defines the extent of the nucleus along the $x^+$ axis. Going to transverse momentum space we have

$$\tilde{s}(\vec{k}_\perp, b^+) = \int d^2 x_\perp e^{-i\vec{k}_\perp \cdot \vec{x}_\perp} s(\vec{x}_\perp, b^+), \tag{4.39}$$

half of the

with $\vec{k}_\perp$ the relative transverse momentum of the quark and the antiquark in the dipole. As we demonstrated above, all the integrations over the minus momenta in the diagrams in Fig. 4.5 are done straightforwardly. Hence the $b^+$-evolution of $\tilde{s}(\vec{k}_\perp, b^+)$ is also clear: in one step in $b^+$ the dipole may interact with one nucleon. Denoting $\tilde{s}(\vec{k}_\perp, b^+)$ by a circle, we illustrate this statement in Fig. 4.10.

138    *Dipole approach to high parton density QCD*

Summing over all possible connections of the $t$-channel gluons to the dipole in Fig. 4.10 we obtain the following equation (Mueller (1990), see also Baier *et al.* (1997)):

$$\frac{\partial \tilde{s}(\vec{k}_\perp, b^+)}{\partial b^+} = -\frac{\rho_A(\vec{b}_\perp, b^+)}{2} \int \frac{d^2 l_\perp}{(2\pi)^2} \frac{d\sigma^0_{qq \to qq}}{d^2 l}$$

$$\times \left[ 2\tilde{s}(\vec{k}_\perp, b^+) - \tilde{s}(\vec{k}_\perp - \vec{l}_\perp, b^+) - \tilde{s}(\vec{k}_\perp + \vec{l}_\perp, b^+) \right], \tag{4.40}$$

where the minus signs outside the last two terms come from the coupling of one gluon to the quark and the other to the antiquark. The differential cross section $d\sigma^0_{qq \to qq}/d^2 l$ is the momentum-space expression for the two-gluon exchange cross section in quark–quark scattering, as given in Eq. (3.18), and the factor $1/2$ is needed to convert it to the forward amplitude. (Again we are modeling the nucleons as single valence quarks.) The nucleon density factor $\rho_A(\vec{b}_\perp, b^+)$ (now, in the boosted-nucleus frame, equal to the number of nucleons per unit volume element $db^+ d^2 b_\perp$) gives the probability of finding a nucleon at a given location in the nucleus. Again we assume $\rho_A(\vec{b}_\perp, b^+)$ to be constant on the perturbatively short transverse distance scales relevant to Eq. (4.40). The overall minus sign in Eq. (4.40) reflects the fact that we are calculating a variation of the $S$-matrix that differs from the variation of the forward amplitude by a sign, as follows from Eq. (4.38).

Fourier-transforming Eq. (4.40) into transverse coordinate space we obtain

$$\frac{\partial s(\vec{x}_\perp, b^+)}{\partial b^+} = -\frac{\rho_A(\vec{b}_\perp, b^+)}{2} \sigma^{q\bar{q}N} s(\vec{x}_\perp, b^+) \tag{4.41}$$

with

$$\sigma^{q\bar{q}N} = \int \frac{d^2 l_\perp}{(2\pi)^2} \frac{d\sigma^0_{qq \to qq}}{d^2 l} \left( 2 - e^{i\vec{l}_\perp \cdot \vec{x}_\perp} - e^{-i\vec{l}_\perp \cdot \vec{x}_\perp} \right), \tag{4.42}$$

exactly the dipole–nucleus cross section of Eqs. (4.25) and (4.28). (The factor 2 difference in comparison to Eq. (4.25) is due to the fact that in Eq. (4.25) the nucleon is modeled as a dipole whereas in our present calculation it is taken to be a single quark for simplicity.)

One can readily see from Eq. (4.41) that in transverse coordinate space Eq. (4.40) becomes trivial. An important consequence of this triviality is that, for the first time, we see explicitly that the transverse size of the dipole $x_\perp$ does not change in the interactions with the nucleons (and the nucleus). This is demonstrates the argument presented in Sec. 4.1.

Equation (4.41) has the following simple physical meaning: as the dipole propagates through the nucleus it may encounter nucleons, with the probability of interaction per unit path length $db^+$ given by the product of the nucleon density $\rho_A$ and half the interaction probability $\sigma^{q\bar{q}N}$ from Eq. (4.28). The initial condition for Eq. (4.41) is given by a freely propagating dipole without interactions, for which $s(\vec{x}_\perp, b^+ = 0) = 1$. Solving Eq. (4.41) with this initial condition yields

$$s(\vec{x}_\perp, b^+) = \exp \left\{ -\int_0^{b^+} db'^+ \frac{\rho_A(\vec{b}_\perp, b'^+)}{2} \sigma^{q\bar{q}N} \right\}. \tag{4.43}$$
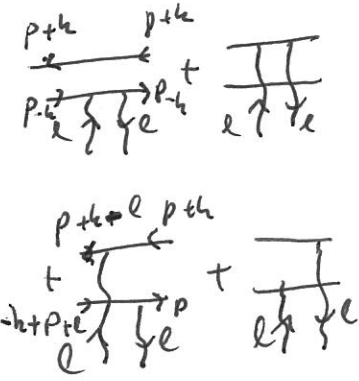
Going back to the nuclear rest frame and remembering that $S(\vec{x}_\perp) = s(\vec{x}_\perp, L)$, we obtain

$$S(\vec{x}_\perp, \vec{b}_\perp, Y = 0) = \exp\left\{-\frac{\sigma^{q\bar{q}N}}{2} T(\vec{b}_\perp)\right\}. \tag{4.44}$$

Note that $\sigma^{q\bar{q}N}$ does not depend on the energy of the collision (and therefore on its net rapidity): to underscore this we have put $Y = 0$ in the argument of the $S$-matrix in Eq. (4.44). This will delineate this expression from the energy-dependent version that results from incorporating small-$x$ evolution into this picture.

Using Eq. (4.44) along with Eq. (4.28) in Eq. (4.38), the imaginary part of the forward scattering amplitude in the Glauber–Gribov–Mueller (GGM) model (Mueller 1990) is given by

$$N(\vec{x}_\perp, \vec{b}_\perp, Y = 0) = 1 - \exp\left\{-\frac{\alpha_s \pi^2}{2N_c} T(\vec{b}_\perp) x_\perp^2 x G_N\left(x, \frac{1}{x_\perp^2}\right)\right\}. \tag{4.45}$$

This is the GGM multiple–rescattering formula. Note again that the nucleon's gluon distribution function $xG_N$ in Eq. (4.45) is taken at the lowest, two-gluon, level and is thus independent of $x$, so that the amplitude $N$ in Eq. (4.45) is independent of energy.

Equation (4.45) has a remarkable property: one can see that it implies $N \leq 1$ for all (perturbative) $x_\perp$. This means that the resulting forward scattering amplitude obeys the black-disk limit constraint (4.33), correcting the problem of the single rescattering amplitude from Eq. (4.32). We see that multiple rescatterings unitarize the scattering cross section, preserving the black-disk limit. The lesson we learn from the Glauber–Gribov–Mueller model is that to unitarize a cross section it is important to include multiple rescatterings!

Equation (4.45) allows us to determine the parameter corresponding to resummation of the diagrams like that shown in Fig. 4.5. Using the gluon distribution from Eq. (4.27) in Eq. (4.45), and noting that for large nuclei the profile function $T(\vec{b}_\perp)$ scales as $A^{1/3}$, we conclude that the resummation parameter of multiple rescatterings is (Kovchegov 1997)

$$\alpha_s^2 A^{1/3}. \tag{4.46}$$

The physical meaning of the parameter $\alpha_s^2 A^{1/3}$ is rather straightforward: at a given impact parameter the dipole interacts with $\sim A^{1/3}$ nucleons, exchanging two gluons with each. Since two-gluon exchange is parametrically of order $\alpha_s^2$ we obtain $\alpha_s^2 A^{1/3}$ as the resummation parameter.

### 4.2.3 Saturation picture from the GGM formula

Multiple nucleon interactions become important in Eq. (4.45) when the dipole size becomes of order $x_\perp \sim 1/Q_s$, where the *saturation* scale $Q_s$ is defined by the following implicit equation (cf. Eq. (3.133)):

$$Q_s^2(\vec{b}_\perp) = \frac{\alpha_s \pi^2}{2N_c} T(\vec{b}_\perp) x G_N(x, Q_s^2). \tag{4.47}$$

Note that for a cylindrical nucleus, as considered in Sec. 3.4.2, one has $T(\vec{b}_\perp) = A/S_\perp$ so that, taking into account that the nuclear gluon distribution is $xG_A = AxG_N$ (which is
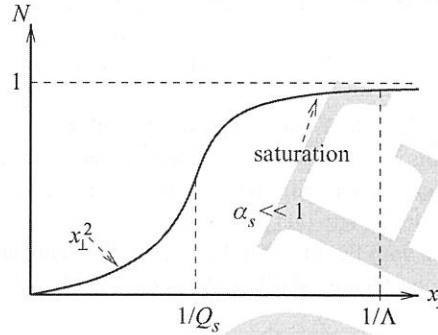
Fig. 4.11. The imaginary part of the forward amplitude of the dipole–nucleus scattering $N$ plotted as a function of the transverse separation between the quark and the anti-quark in a dipole $x_\perp$, using Eq. (4.51). (Reprinted from Jalilian-Marian and Kovchegov (2006), with permission from Elsevier.) A color version of this figure is available online at www.cambridge.org/9780521112574.

true at the two-gluon level considered here), one can recast Eq. (4.47) in almost the exact form of Eq. (3.133). The difference $N_c/C_F$ between the saturation scales in (4.47) and in (3.133) is due to the fact that the saturation scale (4.47) we have just found is that for a quark dipole, whereas the saturation scale in Eq. (3.133) was obtained solely for gluons. If we were to replace the quark dipole in Fig. 4.5 with a gluon dipole, we would need to modify the exponent in Eq. (4.45) by the ratio of the adjoint and fundamental Casimir operators $N_c/C_F$, putting Eq. (4.47) in exact agreement with Eq. (3.133). With this proviso, we see that, at least at the lowest order considered, Eq. (4.47) gives the same saturation scale as what follows from the GLR–MQ equation.

Inserting the lowest-order single-quark gluon distribution function,

$$xG_{LO}^{quark}(x, Q_\perp^2) = \frac{\alpha_s C_F}{\pi} \ln \frac{Q^2}{\Lambda^2}, \tag{4.48}$$

into Eq. (4.45), we can rewrite it as

$$N(\vec{x}_\perp, \vec{b}_\perp, Y = 0) = 1 - \exp\left\{ -\frac{\alpha_s^2 C_F \pi}{N_c} T(\vec{b}_\perp) x_\perp^2 \ln \frac{1}{x_\perp \Lambda} \right\}. \tag{4.49}$$

Defining the quark *saturation* scale (note the factor 4 difference compared with Eq. (4.47) and the absence of a gluon distribution in this definition),

$$Q_s^2(\vec{b}_\perp) \equiv \frac{4\pi \alpha_s^2 C_F}{N_c} T(\vec{b}_\perp), \tag{4.50}$$

we rewrite Eq. (4.49) as

$$N(\vec{x}_\perp, \vec{b}_\perp, Y = 0) = 1 - \exp\left\{ -\frac{x_\perp^2 Q_s^2(\vec{b}_\perp)}{4} \ln \frac{1}{x_\perp \Lambda} \right\}. \tag{4.51}$$

The dipole amplitude $N$ from Eq. (4.51) is plotted schematically in Fig. 4.11 as a function of $x_\perp$. One can see that, at small $x_\perp$, i.e., $x_\perp \ll 1/Q_s$, we have $N \sim x_\perp^2$ so that the amplitude